ACS APPLIED NANO MATERIALS

www.acsanm.org Article

Graphene on Nanoscale-Thick Au Films: Implications for Anticorrosion in Smart Wearable Electronics

Chen-Hsuan Lu, Kuang-Ming Shang, Shi-Ri Lee, Yu-Chong Tai, and Nai-Chang Yeh*

Cite This: https://doi.org/10.1021/acsanm.2c00401 Read Online

ACCESS | Metrics & More | Article Recommendations

ABSTRACT: Gold is normally considered inert to chemical reaction. Nevertheless, as a common electrode material, it would suffer from corrosion when exposed to certain solutions such as sweat and body fluids. Here, we report low-temperature plasma-enhanced chemical vapor deposition (PECVD) of graphene on gold and demonstrate its feasibility for anticorrosion application. The effects of hydrogen-to-methane ratio and the underlying gold substrate on the graphene growth are investigated, and the growth mechanism of PECVD graphene on gold is proposed. When immersed in an oxygenated saline solution, the PECVD-grown graphene-covered gold surface is found to remain intact after an acceleration soaking test at 90 °C for 24 h, which is in contrast to the degradation of bare gold surface subject to the same test. Our findings suggest that consumer/medical wearables and implantable devices with exposed gold can benefit from the protection of a direct, low-temperature PECVD-grown graphene layer for anticorrosion, thereby prolonging the efficacy and reliability of gold electrode-based biosensors.

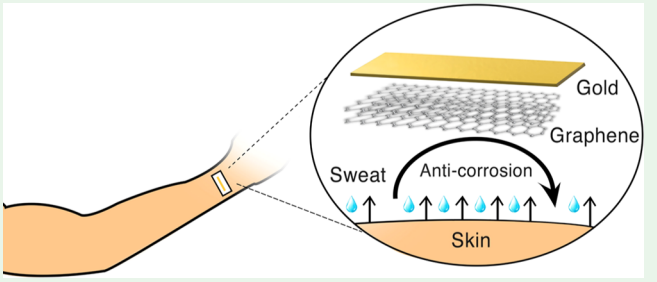

KEYWORDS: *PECVD, graphene, low-temperature, gold, anticorrosion*

1. INTRODUCTION

Since the first successful isolation of monolayer graphene, its unique electronic, optical, and mechanical properties have stimulated a wide range of research activities and applications. Early works of graphene production rely on mechanical exfoliation,[1] which is not scalable for real-world applications. To date, chemical vapor deposition (CVD) is one of the common approaches for large-scale graphene synthesis. Typically, it involves both metallic substrates, such as Ni[2] and Cu,[3] and high growth temperatures to facilitate the dissociation of hydrocarbon precursors for graphene formation.[4] Besides Ni and Cu, other transition metal substrates such as Co,[5] Pt,[6] Au,[7,8] and Ru[9] have been demonstrated for CVD graphene growth.

Gold has been widely adopted in biosensors for its biocompatibility and in flexible electronics for its ductility.[10−12] Despite the common perception that gold is chemically inert for use as electrochemical electrodes, it is still prone to surface oxidation or corrosion.[13,14] Graphene-coated metals have been shown to exhibit enhanced resistance to oxidation,[15] while graphene on gold has been demonstrated to stabilize the Au electrodes for electrochemical application.[16] In addition, graphene coverage on gold could enhance the detection sensitivity of DNA molecules compared to bare gold electrodes.[17] Therefore, graphene could enable versatile applications of gold.

In terms of the growth temperature, CVD graphene growth commonly operates at a temperature near the melting points of the metal foils, which is prone to induce contamination due to evaporated metal and aged quartz furnace.[18] In addition, high-temperature processes would damage substrates that involve polymeric or temperature-sensitive materials, thus limiting their suitability to applications requiring flexible materials.[19] Several approaches have been proposed to lower the graphene growth temperature for thermal CVD. For instance, Jang et al.[20] reported the use of a benzene precursor to reduce the graphene growth temperature to 100 °C, while Fujita et al.[21] demonstrated a near-room temperature graphene growth through liquid metal nucleation. However, these approaches generally involve complicated preprocessing steps that are not compatible with industrial processes for large-area scalable production.[20−22]

On the other hand, plasma-enhanced CVD (PECVD) is a scalable process that could enable low-temperature graphene growth. PECVD relies on plasma to create reactive species to

Received: January 26, 2022
Accepted: February 17, 2022

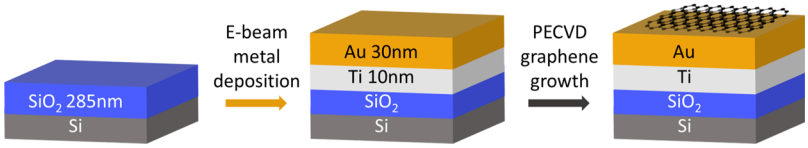

Figure 1. Schematic of the substrate structure along with the subsequent PECVD graphene growth.

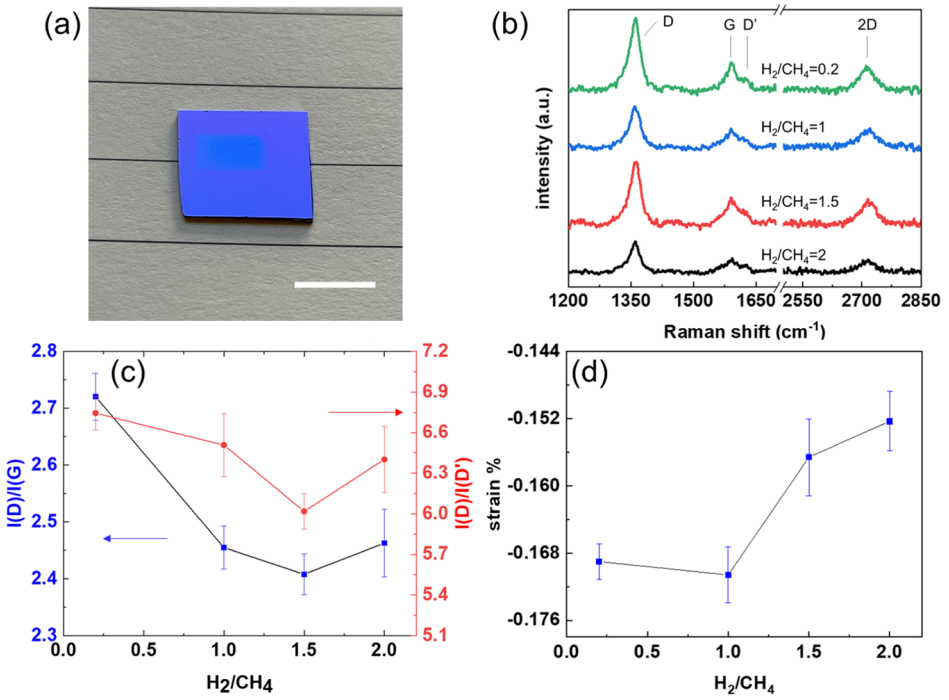

Figure 2. (a) Graphene (lighter blue) transferred onto a SiO_2/Si substrate (darker blue) after its growth on Au/Ti/SiO_2/Si. The scale bar is 1 cm. (b) Raman spectra of PECVD-grown graphene on Au/Ti/SiO_2/Si under different H_2/CH_4 growth conditions. (c) Intensity ratios $I(D)/I(G)$ and $I(D)/I(D')$ extracted from (b). (d) Calculated strain of graphene on Au from eq 2.

lower the required growth temperature. Growth temperature ranging from 160 to 700 °C has been reported for PECVD graphene synthesis on various substrates.[19,23−25] Considering the aforementioned advantages of Au and graphene, as well as the increasing interest in flexible or smart wearable electronics with gold electrodes,[26−29] it is highly desirable to find a method for graphene growth on gold under low temperature.

In this work, we demonstrate the feasibility of direct growth of graphene on gold thin films by PECVD at low temperature. Raman spectroscopy and direct transfer of graphene onto SiO_2 confirm the successful growth of graphene. X-ray diffraction (XRD) studies further reveal that the crystallinity of gold thin films improves after the PECVD graphene growth process. A growth mechanism of PECVD graphene on Au is proposed based on studies of X-ray photoelectron spectroscopy (XPS) and cross-sectional annular dark-field scanning transmission electron microscopy (ADF-STEM) of the PECVD-grown samples. Finally, with accelerated soak testing (AST), we demonstrate excellent anticorrosion performance of graphene on Au. Therefore, our work demonstrates the feasibility of low-temperature direct growth of graphene on gold by PECVD for anticorrosion, paving ways to scalable smart medical applications based on PECVD-grown graphene on gold.

2. EXPERIMENTAL SECTION

2.1. Substrate Preparation. As shown in Figure 1, the Au substrate in this work consists of a Au thin film of 30 nm thickness above a Ti layer of 10 nm thickness, both deposited on a SiO_2/Si substrate with a SiO_2 thickness of 285 nm via an electron-beam (e-beam) evaporator. Prior to metal deposition, the SiO_2/Si wafer was cleaned with the piranha solution, which was a mixture of H_2SO_4:H_2O_2 with a 3:1 volume ratio.

2.2. PECVD Graphene Growth. Prior to the PECVD graphene growth, the quartz tube and sample holders were cleaned with O_2 plasma and H_2 plasma. The plasma system consisted of a microwave generator fixed at 2.45 GHz and an Evenson cavity. Before plasma ignition by a high-frequency coil, CH_4 and H_2 gas were introduced into the quartz tube by mass flow controllers, and the total pressure was set at 750 mTorr, which was controlled by a throttle valve. Here, we define H_2/CH_4 as the ratio of the H_2 gas flow to the CH_4 gas flow. The plasma power was set at 10 W for 5 min and the samples were left to cool down with the gas flow continued after the plasma was turned off. Through plasma heating, the temperature during graphene growth was about 120 °C. To transfer the graphene grown on Au/Ti/SiO_2/Si to a SiO_2/Si substrate, polymethyl methacrylate (PMMA) was spin-coated on the graphene-covered Au/Ti/SiO_2/Si substrates followed by gold etching via a gold etchant (TFA, Transene). Subsequently, the transferred graphene on SiO_2/Si was soaked in acetone for PMMA removal.

2.3. Characterization. After growth, Raman spectroscopy was conducted to confirm the graphene growth and graphene quality. The spectra were collected with a Raman spectrometer (InVia, Renishaw) with 514 nm laser. Surface morphology was characterized by atomic force microscopy (AFM, Bruker Dimension Icon) under the PeakForce tapping mode and scanning electron microscopy (SEM). XPS (Surface Science Instruments MProbe ESCA) with an Al Kα X-ray source and a hemispherical energy analyzer using a pass energy of

https://doi.org/10.1021/acsanm.2c00401
ACS Appl. Nano Mater. XXXX, XXX, XXX−XXX

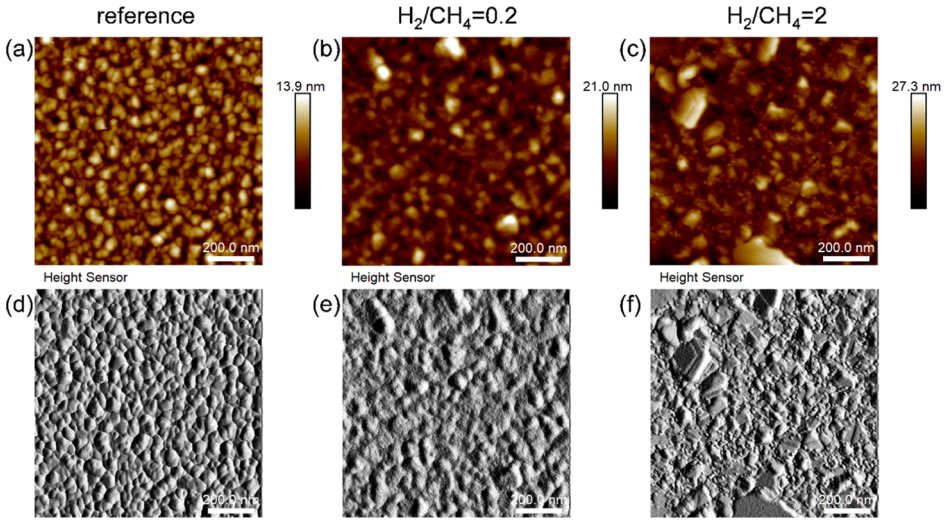

Figure 3. AFM height images and PeakForce error images of the sample surface (a,d) before PECVD, (b,e) after PECVD graphene growth at H_2/CH_4 = 0.2, and (c,f) after PECVD graphene growth at H_2/CH_4 = 2. Here, the scale bar represents 200 nm.

25 eV was used to characterize the chemical change after PECVD. The instrument work function was calibrated with respect to Au $4f_{7/2}$. ADF-STEM images were acquired by aberration-corrected JEOL ARM-200F under 200 kV accelerating voltage. XRD was performed with PANalytical X'Pert PRO with Cu Kα radiation. AST was conducted by immersing the samples of graphene grown on Au/Ti/SiO_2/Si and controlled samples of Au/Ti/SiO_2/Si without graphene into a saline solution (with 0.9% NaCl) for 24 h at 90 °C. The sample edges were sealed with epoxy to prevent from potential reaction of the saline solution with the underlying Ti layer from the edges.

3. RESULTS AND DISCUSSION

Figure 2a shows the optical micrograph image of a graphene sample transferred onto a SiO_2/Si substrate, indicating that graphene had fully covered the Au/Ti/SiO_2/Si substrate of 1 × 0.5 cm^2 despite a short growth time. The Raman spectra of PECVD-grown graphene on Au under different H_2/CH_4 ratios in Figure 2b further confirm the finding of successful graphene growth: The existence of the characteristic Raman modes of graphene (i.e., the D, G, D′, and 2D peaks) clearly indicated successful low-temperature growth of graphene on Au. Specifically, the distinct 2D peak suggested that our PECVD growth process provided significantly better graphene crystallinity than the thermal CVD method, and the latter led to a barely visible 2D peak for a growth temperature of 850 °C.[7] Ani et al.[30] pointed out that the carbon solubility in metal is related to the catalytic activity for hydrocarbon dissociation. The carbon solubility of Au is 0.01%, which is significantly smaller than that of Cu (0.04%) so that CVD growth of graphene on Au is expected to be more difficult than on Cu, consistent with experimental observation.

To further characterize the PECVD-grown graphene on Au, we note that the quality of graphene and its defect types can be inferred from Raman spectroscopic studies through analyzing the intensity ratio of D to G peaks (I(D)/I(G)) and that of D to D′ peaks (I(D)/I(D′)), respectively.[31,32] As shown in Figure 2c, the I(D)/I(G) ratio decreased with increasing H_2/CH_4, which could be attributed to increasing hydrogen radicals that facilitated efficient etching of defective graphene.[33] The quality of the synthesized graphene can be estimated by the D/G ratio through the relation[32]

$$L\ (\mathrm{nm}) = \frac{560}{E_{\mathrm{laser}}^4}\left(\frac{I_{\mathrm{D}}}{I_{\mathrm{G}}}\right)^{-1} \quad (1)$$

where L represents the interdefect distance or the graphene grain size and E_{laser} = 2.41 eV. Using this formula, the graphene grain size was estimated to be ∼6 nm. Although the grain size was not ideal, we found that bilayer graphene with a full coverage over the underlying gold surface could still provide excellent passivation for gold to be elaborated later in this section. This finding may be attributed to the small interlayer spacing of bilayer graphene (<0.35 nm), which effectively prevented most ions from diffusing through the graphene layers to reach the gold surface.

In contrast, the I(D)/I(D′) ratio was consistently between 6 and 7 for all H_2/CH_4 values investigated, which implied primarily vacancy defects in the PECVD-grown graphene on Au.[31]

Quantitatively, the amount of biaxial strain of graphene grown on Au could be derived through the use of the following formula[34]

$$\varepsilon = \frac{\Delta\omega}{2\omega_0\gamma_{2\mathrm{D}}} \quad (2)$$

where $\Delta\omega$ denotes the difference between the Raman shift of the 2D band measured directly on the Au/Ti/SiO_2/Si growth substrate and that measured on the same sample after transferred to a SiO_2/Si substrate, ω_0 is the unstrained (i.e., after transferred to a SiO_2/Si substrate) Raman shift of the 2D band, and γ_{2D} = 3.15 is the Grüneisen parameter of the 2D band.[34] The strain values thus derived from using eq 2 for different H_2/CH_4 ratios are summarized in Figure 2d, which reveal that graphene was compressively strained after direct growth on Au and that the compressive strain became relieved after being transferred to a SiO_2/Si substrate. This finding is in agreement with the previous observation reported by Oznuluer et al.[7]

The decreasing magnitude of compressive strain with increasing H_2/CH_4 as shown in Figure 2d may be attributed to the morphology change illustrated in Figure 3 for images taken using an atomic force microscope. Here, both the height images (Figure 3a−c) and the PeakForce error images (Figure

https://doi.org/10.1021/acsanm.2c00401
ACS Appl. Nano Mater. XXXX, XXX, XXX−XXX

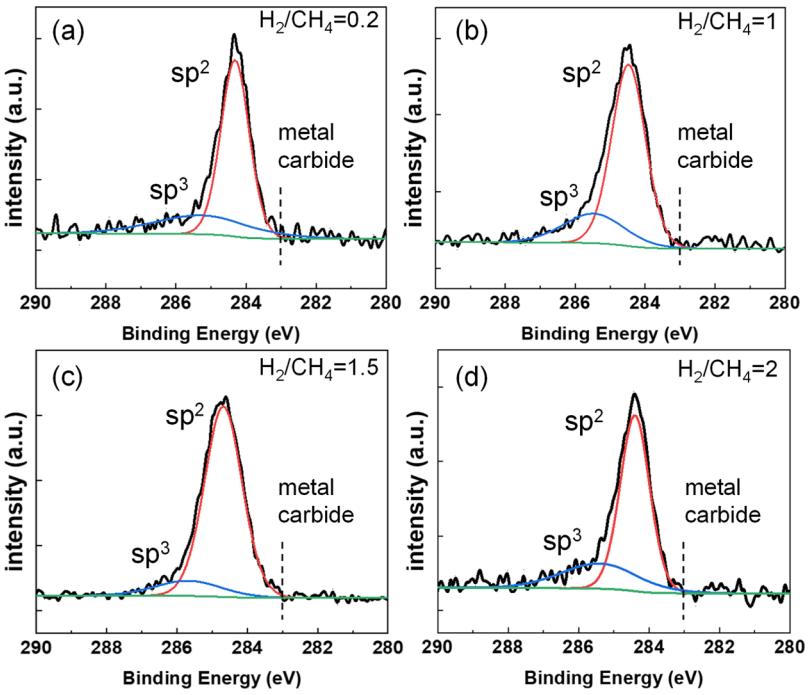

Figure 4. XPS C 1s spectra of the graphene samples after the PECVD process under the growth condition with (a) H_2/CH_4 = 0.2, (b) H_2/CH_4 = 1, (c) H_2/CH_4 = 1.5, and (d) H_2/CH_4 = 2.

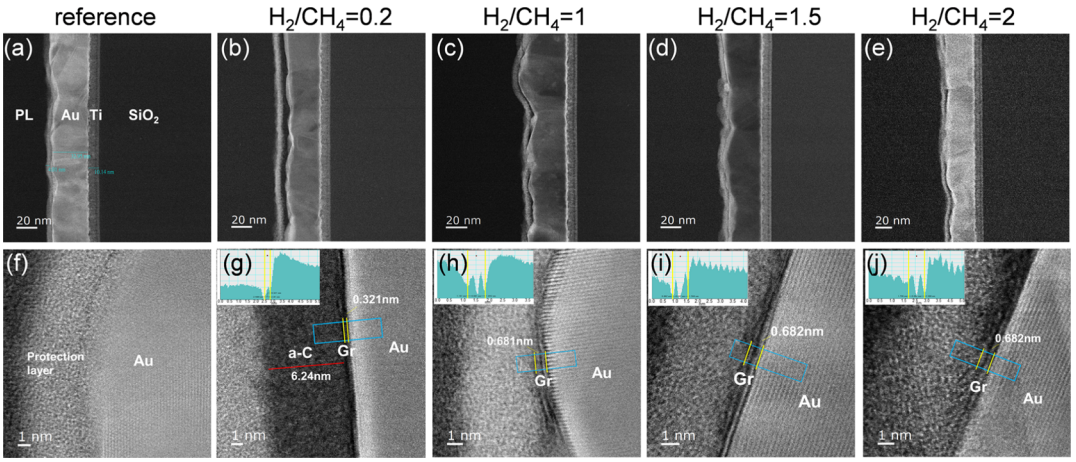

Figure 5. ADF-STEM images at a lower magnification (top row) and higher magnification (bottom row) of (a,f) reference sample without the PECVD process and samples after the PECVD process with the growth condition of (b,g) H_2/CH_4 = 0.2, (c,h) H_2/CH_4 = 1, (d,i) H_2/CH_4 = 1.5, and (e,j) H_2/CH_4 = 2. Here, "PL", "Gr", and "a-C" represent protection layer, graphene, and amorphous carbon, respectively.

3d–f) were included because the PeakForce error images could provide more detailed surface morphology than the height channel.[35]

Before PECVD, the Au surface revealed apparent granular structures (Figure 3a,d), whereas after PECVD graphene growth, the morphology became dependent on the H_2/CH_4 ratio. Comparing the surface morphology for graphene grown under the growth conditions of H_2/CH_4 = 0.2 and H_2/CH_4 = 2, the Au surface under a higher H_2/CH_4 ratio showed smoother surface structures, leading to reduced compressive strain on graphene. The observation of the smoother surface morphology under a higher H_2/CH_4 ratio may be associated with better etching of Au by H_2 plasma.[36]

To elucidate the growth mechanism of graphene on gold by PECVD, measurements of XPS and ADF-STEM were performed. Figure 4 shows the XPS C 1s spectra of the samples after PECVD growth, which further confirmed the formation of graphene on Au from the dominant sp^2 carbon contribution. In addition, the absence of any discernible peak around the binding energy of 283 eV implied that there was no metal carbide formation.[37] The presence of graphene layers under different PECVD growth conditions was further verified by the ADF-STEM images in Figure 5. For H_2/CH_4 = 0.2, we observed mainly monolayer graphene, while for $H_2/CH_4 \geq 1$, we found primarily bilayer graphene. Interestingly, for H_2/CH_4 = 0.2, a clear amorphous carbon layer was also observed while little amorphous carbon was found for $H_2/CH_4 \geq 1$. Based on these experimental findings, we conjecture the PECVD growth mechanism of graphene on Au as schematically illustrated in Figure 6 and further described below.

First, microwave excitation creates a plasma environment with energetic radicals and reacting species that are

https://doi.org/10.1021/acsanm.2c00401
ACS Appl. Nano Mater. XXXX, XXX, XXX−XXX

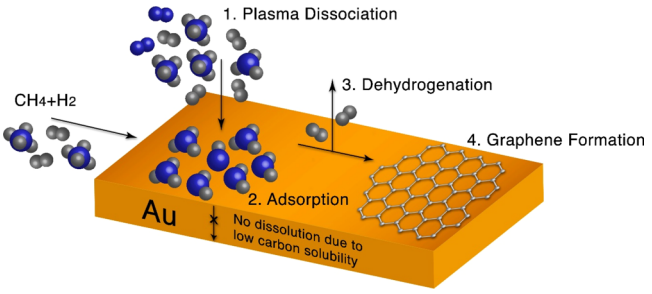

Figure 6. Schematic of the growth mechanism of graphene on gold by PECVD.

dissociated/excited from methane and hydrogen. Plasma also contributes to the heating of the substrates, and the degree of heating depends on the plasma power. Some of the radicals and the hydrocarbon species become adsorbed onto the Au surface, and the dehydrogenation process of the adsorbed hydrocarbon species takes place before carbon radicals migrate and nucleate into graphene. The low carbon solubility in Au limits the number of graphene layers that can be nucleated on the Au surface, and the dehydrogenation and migration processes for graphene formation are dependent on the temperature and the catalytic activity of the substrate. For small H_2/CH_4 ratios (e.g., H_2/CH_4 = 0.2), monolayer graphene formed through the adsorption of carbon species mentioned above. However, further adsorption of carbon species after the nucleation of monolayer graphene led to the formation of an amorphous carbon layer rather than a second layer of graphene. This finding associated with low H_2/CH_4 ratios may be attributed to insufficient hydrogen radicals for etching amorphous carbon[33] and the lower electron temperature of the plasma[19,23] that led to reduced reactivity from the substrate. On the other hand, bilayer graphene without an amorphous carbon layer formed on the Au surface with higher H_2/CH_4 ratios (e.g., $H_2/CH_4 \geq 1$), which may be attributed to the higher substrate reactivity from a higher electron temperature in the plasma[19,23] and sufficient hydrogen radicals for etching amorphous carbon. However, layers beyond bilayer graphene could not be developed due to limited carbon solubility in Au and the hindrance of carbon species to penetrate graphene layers to form the third layer or more.[38] Although plasma significantly reduced the required growth temperature compared to thermal CVD, we note that no graphene growth on Au could take place when the plasma power was lowered from 10 to 8 W, while graphene could still grow on Cu at 8 W.[35] This finding may be attributed to the lower catalytic activity of Au than that of Cu so that a higher substrate temperature or plasma power is required for graphene formation. On the other hand, we note that a high plasma power does not necessarily guarantee successful graphene growth because energetic ion bombardment dominates under a high plasma power, which could lead to significant sample surface damages and removal of adsorbed hydrocarbon species, thus preventing graphene formation.

XRD was conducted to characterize the changes in Au crystallography after the PECVD process, as shown in Figure 7a. The Au(111) intensity counts increased with the H_2/CH_4 ratio and were all much larger than that those without the PECVD process. The extracted Au(111) peak intensity versus H_2/CH_4 ratio is plotted in Figure 7b. Given that our PECVD process was conducted without any active heating source, the increased crystallinity compared to the reference sample could be attributed to plasma activation that provided sufficient thermal energy and that the increased crystallinity with the H_2/CH_4 ratio could be due to the increasing electron temperature of the plasma.[19]

To evaluate if the directly grown graphene on gold could passivate the gold surface, we performed AST by soaking both a bare Au/Ti/SiO_2/Si substrate and a sample of PECVD-grown graphene on Au/Ti/SiO_2/Si into oxygenated saline solution of 0.9% NaCl for 24 h at 90 °C. It is known that body fluids, which may be approximated by the oxygenated saline solution, are highly corrosive to metals.[14,39]

Figure 8 shows the SEM images of the indicated samples after AST and the insets show the optical images before and after AST. Clearly, the sample without graphene coverage exhibited a damaged surface, while the surface for the graphene-covered sample remained intact. In addition, the AST (under 90 °C for 24 h) adapted in our work was equivalent to the condition of approximately 1 month under normal human body temperature.[14,40] Therefore, our demonstration of graphene-provided protection of gold films in an oxygenated saline solution at 90 °C for 24 h is sufficient for such medical applications as disposable wearable sensors. On the other hand, although samples synthesized with a ratio of H_2/CH_4 = 0.2 were monolayer graphene, the amorphous carbon above the graphene layer contributed to enhancing the efficiency of these samples for passivation. On the other hand, for samples synthesized with higher H_2/CH_4 ratios, the resulting bilayer graphene structure made it difficult for ions to diffuse through the layers of a very small interlayer spacing to reach the gold surface. Therefore, excellent passivation could be achieved for samples synthesized with a range of different H_2/CH_4 ratios, as exemplified in Figure 8b for a

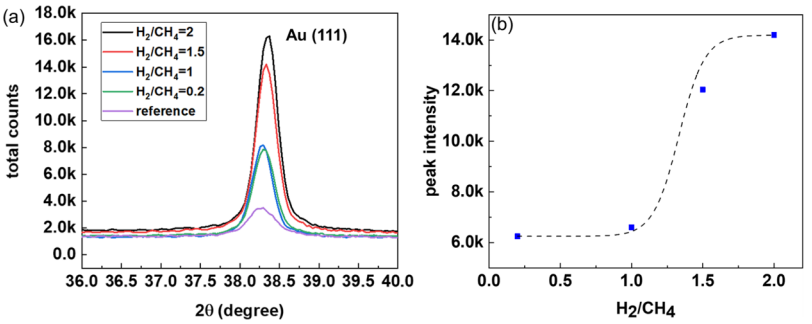

Figure 7. (a) XRD of Au(111) region and (b) extracted Au(111) peak intensity plotted versus H_2/CH_4 ratio. Note that the dashed line is for guidance only.

https://doi.org/10.1021/acsanm.2c00401
ACS Appl. Nano Mater. XXXX, XXX, XXX−XXX

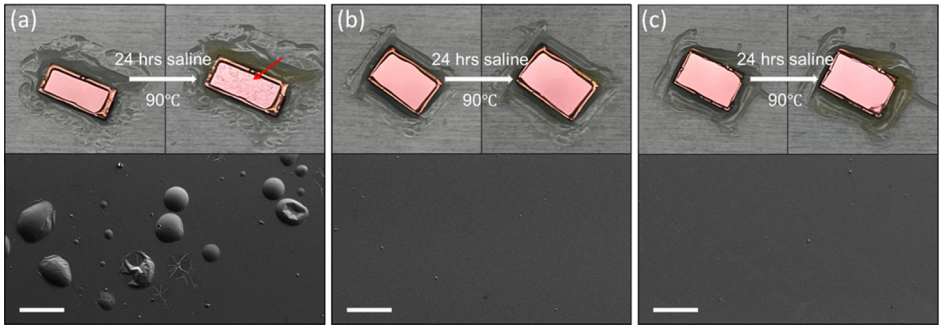

Figure 8. (a) Reference sample without graphene coverage. The red arrow indicates the damaged surface with bubbles. (b) Sample with PECVD graphene coverage grown under the condition $H_2/CH_4 = 0.2$. (c) Sample with PECVD graphene coverage grown under the condition $H_2/CH_4 = 2$. The top row shows the optical images before and after AST. The bottom row shows the SEM images taken after AST. The scale bar is 100 μm.

sample synthesized under the condition of $H_2/CH_4 = 0.2$ and in Figure 8c for a sample synthesized under the condition of $H_2/CH_4 = 2$.

4. CONCLUSIONS

In conclusion, we reported low-temperature graphene growth directly on gold by PECVD. Raman spectroscopic studies showed that PECVD-grown graphene underwent a compressive strain on Au and that the defects in the graphene were mainly vacancies. The surface morphology and crystallinity of Au was investigated using AFM and XRD, respectively, and was found to be dependent on the H_2/CH_4 ratio used during the PECVD process. ADF-STEM images also verified that the number of graphene layers grown on Au was related to the growth condition of the H_2/CH_4 ratio. A growth mechanism of graphene on Au is proposed based on XPS and ADF-STEM studies of the PECVD-grown samples. Finally, excellent anticorrosion performance of graphene on Au was demonstrated by AST in oxygenated saline solution. Therefore, our work of low-temperature direct growth of graphene on gold by PECVD appears promising for anticorrosion in smart wearable, implantable, and flexible hybrid electronics.

AUTHOR INFORMATION

Corresponding Author

Nai-Chang Yeh − *Department of Physics, California Institute of Technology, Pasadena, California 91125, United States;* orcid.org/0000-0002-1826-419X; Email: ncyeh@caltech.edu

Authors

Chen-Hsuan Lu − *Department of Applied Physics and Materials Science, California Institute of Technology, Pasadena, California 91125, United States;* orcid.org/0000-0002-4802-1332

Kuang-Ming Shang − *Department of Medical Engineering, California Institute of Technology, Pasadena, California 91125, United States;* orcid.org/0000-0001-5065-7607

Shi-Ri Lee − *Department of Electron Microscopy Development and Application, Division of Platform Technology for Advanced Materials, Material and Chemical Research Laboratories, Industrial Technology Research Institute, Hsinchu 31057, Taiwan*

Yu-Chong Tai − *Department of Medical Engineering and Department of Electrical Engineering, California Institute of Technology, Pasadena, California 91125, United States*

Complete contact information is available at: https://pubs.acs.org/10.1021/acsanm.2c00401

Author Contributions

The project was conceived jointly by C.-H.L. and N.-C.Y. C.-H.L. performed the graphene growth, Raman spectroscopic studies, and XPS and AFM measurements. K.-M. S. prepared the gold substrates and performed SEM imaging and AST test. S.-R. L. performed the ADF-STEM studies. N.-C. Y. and Y.-C. T. coordinated the research activities at Caltech. The manuscript was written with contributions from all authors. All authors have approved the final version of the manuscript.

Funding

This work is supported by the Industrial Technology Research Institute (ITRI) in Taiwan (NCY.PECVD2-1-ITRI.SRA2021).

Notes

The authors declare no competing financial interest.

ACKNOWLEDGMENTS

C.-H.L. acknowledges Professor George Rossman for providing access to the Raman spectrometer and the Molecular Materials Research Center in the Beckman Institute of the Caltech for access to XPS and AFM. C.-H.L. thanks Dr. Wei-Hsiang Lin for discussion on XPS results and acknowledges Dr. Chyi-Ming Leu at the Material and Chemical Research Laboratories (MCL) in ITRI for coordinating the STEM imaging and XRD acquisition. C.-H.L and K.-M.S. acknowledge the support from the J. Yang & Family Foundation.

REFERENCES

(1) Novoselov, K. S.; Geim, A. K.; Morozov, S. V.; Jiang, D.; Zhang, Y.; Dubonos, S. V.; Grigorieva, I. V.; Firsov, A. A. Electric Field Effect in Atomically Thin Carbon Films. *Science* **2004**, *306*, 666−669.

(2) Kim, K. S.; Zhao, Y.; Jang, H.; Lee, S. Y.; Kim, J. M.; Kim, K. S.; Ahn, J.-H.; Kim, P.; Choi, J.-Y.; Hong, B. H. Large-Scale Pattern Growth of Graphene Films for Stretchable Transparent Electrodes. *Nature* **2009**, *457*, 706−710.

(3) Li, X.; Cai, W.; An, J.; Kim, S.; Nah, J.; Yang, D.; Piner, R.; Velamakanni, A.; Jung, I.; Tutuc, E.; Banerjee, S. K.; Colombo, L.; Ruoff, R. S. Large-Area Synthesis of High-Quality and Uniform Graphene Films on Copper Foils. *Science* **2009**, *324*, 1312−1314.

(4) Liu, W.; Li, H.; Xu, C.; Khatami, Y.; Banerjee, K. Synthesis of High-quality Monolayer and Bilayer Graphene on Copper Using Chemical Vapor Deposition. *Carbon* **2011**, *49*, 4122.

(5) Ramón, M. E.; Gupta, A.; Corbet, C.; Ferrer, D. A.; Movva, H. C. P.; Carpenter, G.; Colombo, L.; Bourianoff, G.; Doczy, M.; Akinwande, D.; Tutuc, E.; Banerjee, S. K. CMOS-Compatible Synthesis of Large-Area, High-Mobility Graphene by Chemical

Vapor Deposition of Acetylene on Cobalt Thin Films. *ACS Nano* **2011**, *5*, 7198−7204.
(6) Kang, B. J.; Mun, J. H.; Hwang, C. Y.; Cho, B. J. Monolayer Graphene Growth on Sputtered Thin Film Platinum. *J. Appl. Phys.* **2009**, *106*, 104309.
(7) Oznuluer, T.; Pince, E.; Polat, E. O.; Balci, O.; Salihoglu, O.; Kocabas, C. Synthesis of Graphene on Gold. *Appl. Phys. Lett.* **2011**, *98*, 183101.
(8) Terasawa, T.-o.; Taira, T.; Yasuda, S.; Obata, S.; Saiki, K.; Asaoka, H. Effect of Hydrogen on Chemical Vapor Deposition Growth of Graphene on Au Substrates. *Jpn. J. Appl. Phys.* **2019**, *58*, SIIB17.
(9) Sutter, P.; Ciobanu, C. V.; Sutter, E. Real-Time Microscopy of Graphene Growth on Epitaxial Metal Films: Role of Template Thickness and Strain. *Small* **2012**, *8*, 2250−2257.
(10) Li, Y.; Schluesener, H. J.; Xu, S. Gold Nanoparticle-Based Biosensors. *Gold Bull.* **2010**, *43*, 29−41.
(11) Khan, Y.; Pavinatto, F. J.; Lin, M. C.; Liao, A.; Swisher, S. L.; Mann, K.; Subramanian, V.; Maharbiz, M. M.; Arias, A. C. Inkjet-Printed Flexible Gold Electrode Arrays for Bioelectronic Interfaces. *Adv. Funct. Mater.* **2016**, *26*, 1004−1013.
(12) Ferrario, A.; Scaramuzza, M.; Pasqualotto, E.; De Toni, A.; Paccagnella, A. Development of a Disposable Gold Electrodes-Based Sensor for Electrochemical Measurements of cDNA Hybridization. *Procedia Chem.* **2012**, *6*, 36−45.
(13) Brummer, S. B.; Makrides, A. C. Surface Oxidation of Gold Electrodes. *J. Electrochem. Soc.* **1964**, *111*, 1122.
(14) Li, W.; Rodger, D. C.; Meng, E.; Weiland, J. D.; Humayun, M. S.; Tai, Y.-C. Wafer-Level Parylene Packaging With Integrated RF Electronics for Wireless Retinal Prostheses. *J. Microelectromech. Syst.* **2010**, *19*, 735−742.
(15) Chen, S.; Brown, L.; Levendorf, M.; Cai, W.; Ju, S.-Y.; Edgeworth, J.; Li, X.; Magnuson, C. W.; Velamakanni, A.; Piner, R. D.; Kang, J.; Park, J.; Ruoff, R. S. Oxidation Resistance of Graphene-Coated Cu and Cu/Ni Alloy. *ACS Nano* **2011**, *5*, 1321−1327.
(16) Yasuda, S.; Kumagai, R.; Nakashima, K.; Murakoshi, K. Electrochemical Potential Stabilization of Reconstructed Au(111) Structure by Monolayer Coverage with Graphene. *J. Phys. Chem. Lett.* **2015**, *6*, 3403−3409.
(17) Song, B.; Li, D.; Qi, W.; Elstner, M.; Fan, C.; Fang, H. Graphene on Au(111): A Highly Conductive Material with Excellent Adsorption Properties for High-Resolution Bio/Nanodetection and Identification. *ChemPhysChem* **2010**, *11*, 585−589.
(18) Lisi, N.; Dikonimos, T.; Buonocore, F.; Pittori, M.; Mazzaro, R.; Rizzoli, R.; Marras, S.; Capasso, A. Contamination-Free Graphene by Chemical Vapor Deposition in Quartz Furnaces. *Sci. Rep.* **2017**, *7*, 9927.
(19) Lu, C.-H.; Leu, C.-M.; Yeh, N.-C. Single-Step Direct Growth of Graphene on Cu Ink toward Flexible Hybrid Electronic Applications by Plasma-Enhanced Chemical Vapor Deposition. *ACS Appl. Mater. Interfaces* **2021**, *13*, 6951−6959.
(20) Jang, J.; Son, M.; Chung, S.; Kim, K.; Cho, C.; Lee, B. H.; Ham, M.-H. Low-Temperature-Grown Continuous Graphene Films from Benzene by Chemical Vapor Deposition at Ambient Pressure. *Sci. Rep.* **2015**, *5*, 17955.
(21) Fujita, J.-i.; Hiyama, T.; Hirukawa, A.; Kondo, T.; Nakamura, J.; Ito, S.-i.; Araki, R.; Ito, Y.; Takeguchi, M.; Pai, W. W. Near Room Temperature Chemical Vapor Deposition of Graphene with Diluted Methane and Molten Gallium Catalyst. *Sci. Rep.* **2017**, *7*, 12371.
(22) Kwak, J.; Chu, J. H.; Choi, J.-K.; Park, S.-D.; Go, H.; Kim, S. Y.; Park, K.; Kim, S.-D.; Kim, Y.-W.; Yoon, E.; Kodambaka, S.; Kwon, S.-Y. Near Room-Temperature Synthesis of Transfer-Free Graphene Films. *Nat. Commun.* **2012**, *3*, 645.
(23) Boyd, D. A.; Lin, W.-H.; Hsu, C.-C.; Teague, M. L.; Chen, C.-C.; Lo, Y.-Y.; Chan, W.-Y.; Su, W.-B.; Cheng, T.-C.; Chang, C.-S.; Wu, C.-I.; Yeh, N.-C. Single-Step Deposition of High-Mobility Graphene at Reduced Temperatures. *Nat. Commun.* **2015**, *6*, 6620.
(24) Terasawa, T.-o.; Saiki, K. Growth of Graphene on Cu by Plasma Enhanced Chemical Vapor Deposition. *Carbon* **2012**, *50*, 869−874.
(25) Guo, L.; Zhang, Z.; Sun, H.; Dai, D.; Cui, J.; Li, M.; Xu, Y.; Xu, M.; Du, Y.; Jiang, N.; Huang, F.; Lin, C.-T. Direct Formation of Wafer-Scale Single-Layer Graphene Films on the Rough Surface Substrate by PECVD. *Carbon* **2018**, *129*, 456−461.
(26) Jeerapan, I.; Poorahong, S. Review—Flexible and Stretchable Electrochemical Sensing Systems: Materials, Energy Sources, and Integrations. *J. Electrochem. Soc.* **2020**, *167*, 037573.
(27) Li, Z.; Wang, G.; Li, Z.; Cheng, Z.; Zhou, G.; Li, S. Flexible Transparent Electrodes Based on Gold Nanomeshes. *Nanoscale Res. Lett.* **2019**, *14*, 132.
(28) Ling, Y.; Lyu, Q.; Zhai, Q.; Zhu, B.; Gong, S.; Zhang, T.; Dyson, J.; Cheng, W. Design of Stretchable Holey Gold Biosensing Electrode for Real-Time Cell Monitoring. *ACS Sens.* **2020**, *5*, 3165−3171.
(29) Wang, R.; Zhai, Q.; An, T.; Gong, S.; Cheng, W. Stretchable Gold Fiber-Based Wearable Textile Electrochemical Biosensor for Lactate Monitoring in Sweat. *Talanta* **2021**, *222*, 121484.
(30) Ani, M. H.; Kamarudin, M. A.; Ramlan, A. H.; Ismail, E.; Sirat, M. S.; Mohamed, M. A.; Azam, M. A. A Critical Review on the Contributions of Chemical and Physical Factors toward the Nucleation and Growth of Large-Area Graphene. *J. Mater. Sci.* **2018**, *53*, 7095−7111.
(31) Eckmann, A.; Felten, A.; Mishchenko, A.; Britnell, L.; Krupke, R.; Novoselov, K. S.; Casiraghi, C. Probing the Nature of Defects in Graphene by Raman Spectroscopy. *Nano Lett.* **2012**, *12*, 3925−3930.
(32) Dresselhaus, M. S.; Jorio, A.; Souza Filho, A. G.; Saito, R. Defect Characterization in Graphene and Carbon Nanotubes using Raman Spectroscopy. *Philos. Trans. R. Soc., A* **2010**, *368*, 5355−5377.
(33) Vlassiouk, I.; Regmi, M.; Fulvio, P.; Dai, S.; Datskos, P.; Eres, G.; Smirnov, S. Role of Hydrogen in Chemical Vapor Deposition Growth of Large Single-Crystal Graphene. *ACS Nano* **2011**, *5*, 6069.
(34) Jiang, T.; Wang, Z.; Ruan, X.; Zhu, Y. Equi-Biaxial Compressive Strain in Graphene: Grüneisen Parameter and Buckling Ridges. *2D Materials* **2018**, *6*, 015026.
(35) Lu, C.-H.; Leu, C.-M.; Yeh, N.-C. Polymer-Compatible Low-Temperature Plasma-Enhanced Chemical Vapor Deposition of Graphene on Electroplated Cu for Flexible Hybrid Electronics. *ACS Appl. Mater. Interfaces* **2021**, *13*, 41323−41329.
(36) Green, T. A. Gold Etching for Microfabrication. *Gold Bull.* **2014**, *47*, 205−216.
(37) Wiltner, A.; Linsmeier, C. Formation of Endothermic Carbides on Iron and Nickel. *Phys. Status Solidi A* **2004**, *201*, 881−887.
(38) Lee, H. C.; Liu, W.-W.; Chai, S.-P.; Mohamed, A. R.; Aziz, A.; Khe, C.-S.; Hidayah, N. M. S.; Hashim, U. Review of the Synthesis, Transfer, Characterization and Growth Mechanisms of Single and Multilayer Graphene. *RSC Adv.* **2017**, *7*, 15644−15693.
(39) Kamachimudali, U.; Sridhar, T. M.; Raj, B. Corrosion of Bio Implants. *Sadhana* **2003**, *28*, 601−637.
(40) Janting, J.; Theander, J. G.; Egesborg, H. On Thermal Acceleration of Medical Device Polymer Aging. *IEEE Trans. Device Mater. Reliab.* **2019**, *19*, 313−321.

https://doi.org/10.1021/acsanm.2c00401
ACS Appl. Nano Mater. XXXX, XXX, XXX−XXX